seconds or less. These impulsive variations are clearly indicated by the large ratio of the peak to average field strengths evident in Fig. 2. The highly inhomogeneous structure indicated by these variations was not contemplated in the original model of Ginzburg and Zheleznyakov, which only dealt with the linear growth of the plasma oscillations, and has been studied only recently (*5*) in relation to the large-amplitude nonlinear evolution of the two-stream instability. Considerable further investigation, both theoretical and experimental, is still required to fully understand the spatial structure of these intense plasma oscillations and the implications with regard to the generation of radio emissions by the sun and other cosmic radio sources.

DONALD A. GURNETT
ROGER R. ANDERSON
*Department of Physics and Astronomy, University of Iowa, Iowa City 52242*

**References and Notes**

1. V. L. Ginzburg and V. V. Zheleznyakov, *Sov. Astron. AJ* **2**, 653 (1958).
2. J. P. Wild, *Aust. J. Sci. Res. Ser. A* **3**, 541 (1950).
3. L. A. Frank and D. A. Gurnett, *Sol. Phys.* **27**, 446 (1972); H. Alvarez, F. Haddock, R. P. Lin, *ibid.* **26**, 468 (1972); R. P. Lin, L. G. Evans, J. Fainberg, *Astrophys. Lett.* **14**, 191 (1973).
4. P. A. Sturrock, *Nature (London)* **192**, 58 (1961); D. A. Tidman, T. J. Birmingham, H. M. Stainer, *Astrophys. J.* **146**, 207 (1966); S. A. Kaplan and V. N. Tsytovich, *Sov. Astron. AJ* **11**, 956 (1968); D. F. Smith, *Space Sci. Rev.* **16**, 91 (1974).
5. K. Papadopoulos, M. L. Goldstein, R. A. Smith, *Astrophys. J.* **190**, 175 (1974).
6. M. L. Kaiser, *Sol. Phys.* **35**, 181 (1975).
7. D. A. Gurnett and L. A. Frank, *ibid.*, p. 477.
8. F. L. Scarf, R. W. Fredricks, L. A. Frank, M. Neugebauer, *J. Geophys. Res.* **76**, 5162 (1971).
9. D. A. Gurnett and R. R. Anderson, *ibid.*, in press.
10. We thank H. Rosenbauer and R. Schwenn from the Max-Planck-Institut for providing the plasma density data from Helios.
11. Research at the University of Iowa was supported by NASA contract NAS5-11279 and grant NGL-16-001-043. Research was performed by D.A.G. while on leave at the Max-Planck-Institut für Extraterrestrische Physik, Garching bei München, West Germany. Research at the Max-Planck-Institut was supported by the Alexander von Humboldt Foundation.

14 July 1976; revised 8 October 1976

## Elemental Analysis of Biological Specimens in Air with a Proton Microprobe

Abstract. *The unique capabilities of the proton microprobe in an atmospheric environment as a biological tool are illustrated in studies of arsenic and mercury distributions in single strands of hair from poisoning victims and of the distributions of several abundant elements in frozen hydrated eye and kidney specimens from rats.*

In an earlier report (*1*) we described the capabilities of the scanning proton microprobe to map out the spatial distributions of a given element (or elements), even at trace concentrations, using a 2-Mev collimated proton microbeam emergent into air. With this technique, the sample is mechanically scanned in front of the stationary microbeam while an energy-dispersive x-ray detector collects proton-induced x-rays characteristic of the elemental species being excited by the microbeam at each instant. This information can be displayed on a conventional oscilloscope if the trace is moved in synchronization with the sample motion, brightening the spot when x-rays of a particular energy are detected; alternatively, the information can be stored in a multichannel scaler or computer memory for subsequent analysis. The latter procedure is particularly convenient when a one-dimensional scan is made repeatedly across a sample, since one obtains a graph of the abundance of each element versus position along the scan direction. We have found this method of a linear scan useful for obtaining quantitative data about a sample which has shown interesting features in a two-dimensional scanning micrograph; this technique is also the obvious method for examining one-dimensional samples, for example, strands of hair. Samples need not be cut into thin sections but may be prepared arbitrarily thick, since the proton microprobe detects x-rays emitted only from the top 25 to 50 $\mu$m of the specimen. We illustrate here the application of this technique to (i) trace element distributions in single strands of hair and (ii) electrolyte distributions in frozen hydrated eye and kidney specimens.

The measurement of trace element concentrations in hair or nail tissue as a function of distance along the growth direction can provide a measure of the body's uptake of heavy metals or other relatively rare chemical constituents as a function of time; it may also reflect biochemical changes in the whole organism. The techniques of chemical analysis, atomic absorption spectroscopy, and neutron activation (*2*) have been used to determine the trace element content in short lengths of hair or nail tissue analyzed separately; these methods exhibit poor spatial resolution and insensitivity to certain elements. What is needed is a simple nondestructive method, sensitive to many elements simultaneously, with good spatial resolution. Major advances in this direction have been made with the use of electron microprobe analysis and x-ray fluorescence (XRF) analysis (*3*).

The scanning proton microprobe, with its intense collimated beam and low background signal, combines some of the advantages of both techniques, allowing one to analyze a single strand of hair with high spatial resolution (corresponding to a fraction of a day's growth), and high sensitivity simultaneously for most elements heavier than sodium (*4*). Because of the difficulty of aligning separate hairs and because of variations in the growth rate of individual hairs (*5, 6*), it is essential that only a single strand of hair be used if high spatial resolution is to be attained. We have analyzed hairs from an individual poisoned by ingesting methylmercury-treated seed grain in Iraq and from a victim of accidental arsine inhalation (*7*). The technique is straightforward: a hair is cemented to a rigid strip of Kapton with Kodak Micro Resist 747 (both materials are radiation-resistant, stable at high temperature, and relatively free of heavy element contamination), then scanned repeatedly past the proton microbeam by a lead screw assembly driven by a stepping motor. Proton-induced x-rays corresponding to each element of interest are detected and stored in a multichannel analyzer as a function of sample position. Thus one simultaneously obtains graphs of the abundance of a number of elements versus position along the hair. Typically, a current of 5 na of 2-Mev protons collimated to a beam diameter of 100 to 150 $\mu$m is used.

Figure 1a shows arsenic and zinc distributions obtained in this way from a strand of hair taken from the arsine-poisoned patient 183 days after inhalation. The arsenic peak is about 0.15 cm wide (corresponding to 5.1 days), located approximately 5.6 cm from the root. A simultaneous drop in the zinc content is followed by a slower recovery (25 days) to normal concentrations, an effect not previously reported to our knowledge. The iron concentration does not change, demonstrating that the zinc effect is not an artifact of the technique. Another hair taken from the patient 19 days after inhalation showed an almost identical pattern, both in the peak arsenic content and the corresponding drop in the zinc content. On the basis of several methods of calibration, we estimate the peak arsenic concentration to be $\sim$ 200 $\mu$g/g.

Successive 1-cm hair segments taken at the same two times were also studied by

neutron activation analysis; peak arsenic concentrations of 33 and 107 $\mu$g/g, respectively, were measured (*8*). Although this large difference between the two samples is not consistent with the proton microprobe data, which shows the peak arsenic contents to be nearly identical ($\pm$ 10 percent), it is not surprising that the maximum values of the arsenic content determined by neutron activation are smaller than ours, since they represent 1-cm averages of peaks which Fig.

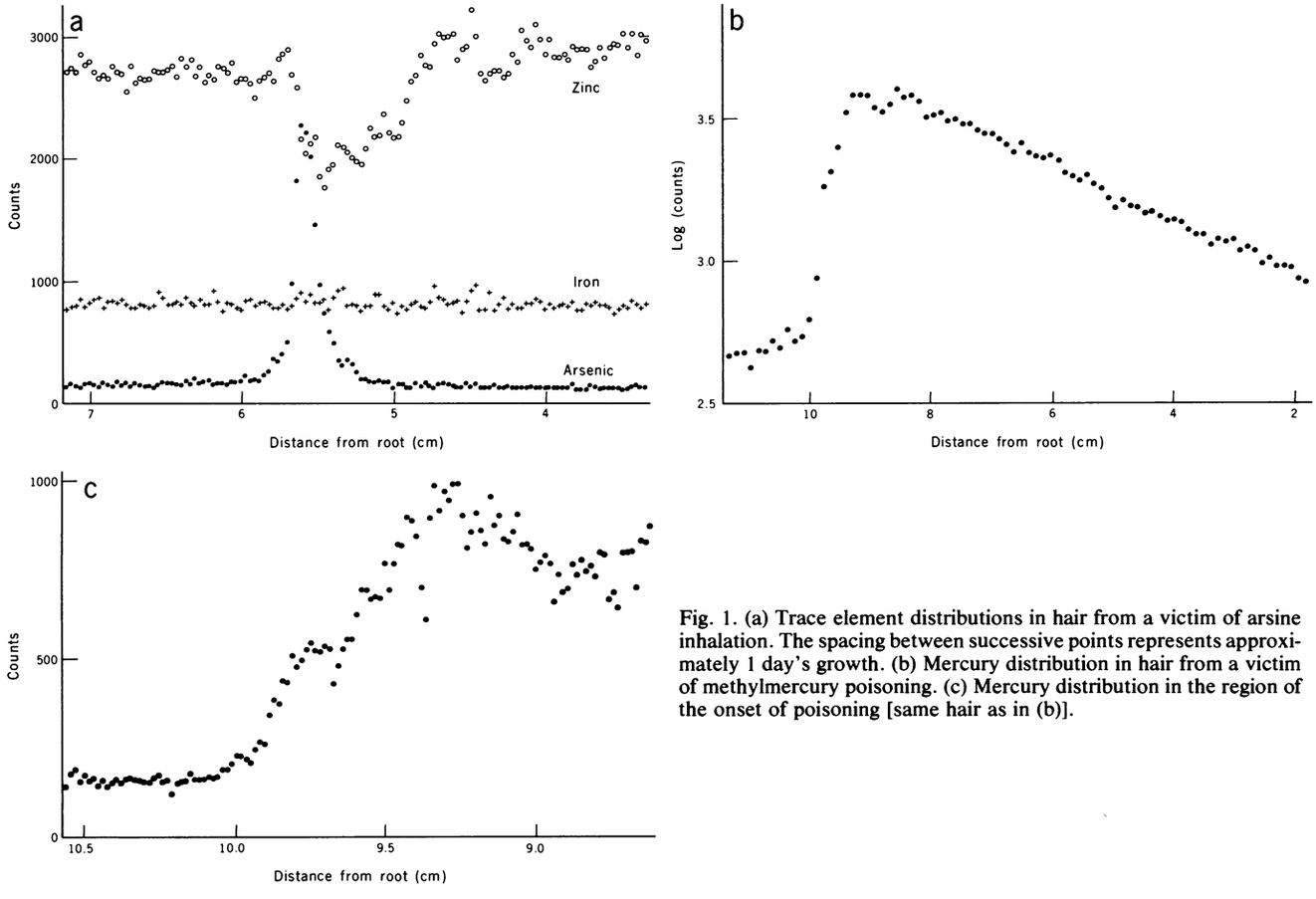


Fig. 1. (a) Trace element distributions in hair from a victim of arsine inhalation. The spacing between successive points represents approximately 1 day's growth. (b) Mercury distribution in hair from a victim of methylmercury poisoning. (c) Mercury distribution in the region of the onset of poisoning [same hair as in (b)].

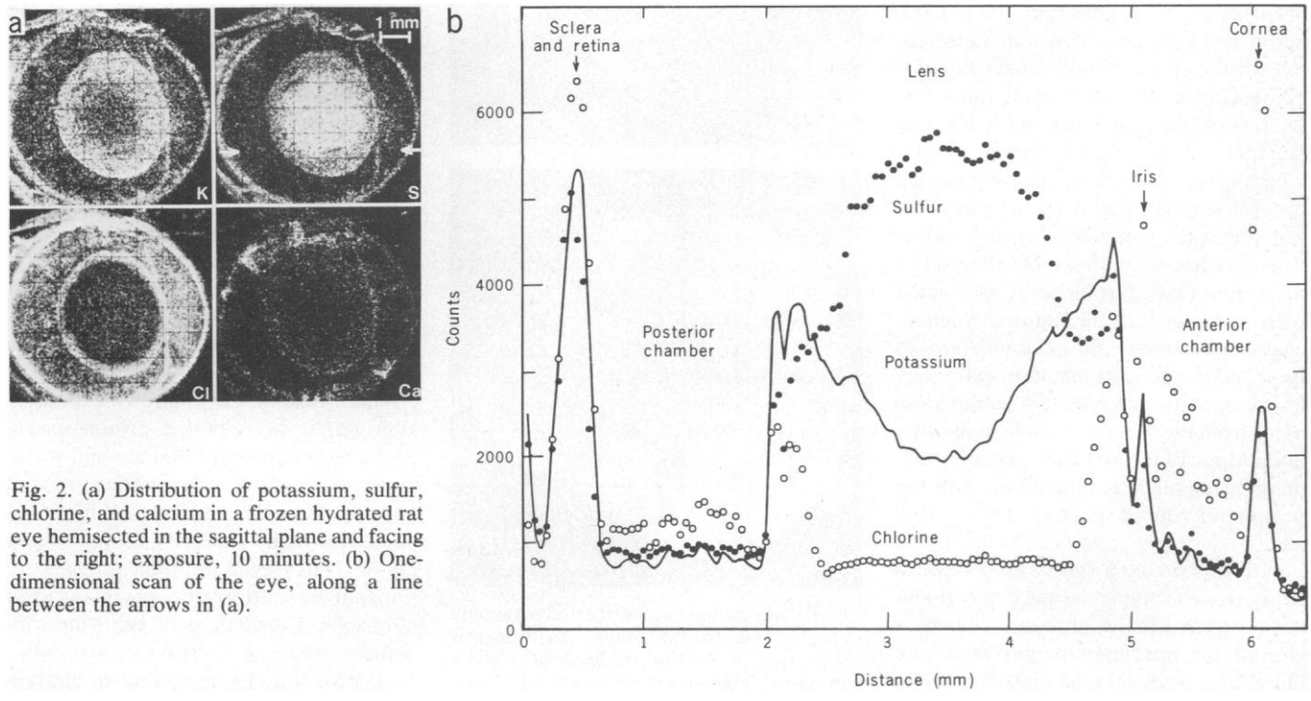


Fig. 2. (a) Distribution of potassium, sulfur, chlorine, and calcium in a frozen hydrated rat eye hemisected in the sagittal plane and facing to the right; exposure, 10 minutes. (b) One-dimensional scan of the eye, along a line between the arrows in (a).

1a shows to be considerably narrower than 1 cm.

A strand of hair from a victim of methylmercury poisoning was also analyzed with the proton microprobe, with the results shown in Fig. 1b. By comparison with the case for arsenic, the mercury content of the hair falls off slowly, with an exponential decay distance of 4.5 cm [approximately 4 months, assuming a growth rate of 0.37 mm/day (*6*)]. No correlation with zinc content was observed. Figure 1c, which shows the region where the mercury content rises in greater detail, suggests a history of several ingestions of mercury. Hair samples for several centimeters earlier than the section graphed here (that is, to the left of the graph) showed only background concentrations of mercury. Other strands of hair from this individual produced nearly identical graphs. Earlier measurements of mercury content as a function of length for hair samples from the Iraq incident, obtained by atomic absorption or XRF analysis (*5*, *9*), show considerably slower rise times, typically 2 to 4 cm; this difference may be due to different histories of ingestion, or to the difficulty of aligning the multiple strands of hair used in earlier studies.

For a variety of studies it is essential that the specimens be examined in the hydrated state. A central problem in biology is understanding the mechanisms of compartmentalization of mobile ions. Only living or frozen hydrated specimens accurately maintain the physiological distributions of diffusible ions; analytical techniques involving the use of freeze-drying, embedding, and precipitation are likely to result in major elemental redistributions (*10*). Analyzing hydrated specimens provides count rates that are related in a simple manner to local elemental concentration in the wet tissue, a parameter of physiological importance not measurable by other techniques. Frozen stages are being developed for electron microprobe analysis, but they suffer from the practical difficulties associated with sample transfer into a vacuum chamber without the accumulation of frost and the need to maintain extremely low temperatures to prevent sublimation of ice from the specimen while in the vacuum. Much of the awkwardness of a vacuum frozen stage is eliminated with the proton microprobe, which operates in air.

We constructed a simple cold stage to study frozen samples of rat eye and kidney tissue. Liquid nitrogen circulates around the specimen mount at a rate more than sufficient to cool the stage, and a thermistor-controlled heating element then stabilizes the temperature at a selected value, typically −30°C. At this temperature diffusible substances are immobilized on the scale of resolution employed in these experiments (≈ 100 μm), as demonstrated by the sharp detail and the stability of the results over several hours. Frost formation was prevented by sealing the specimen in a small chamber behind a 7-μm Kapton film, upon which a stream of dry nitrogen is blown. (One could instead surround the sample, stage, detector, and beam hardware with a flexible plastic hood maintained under positive pressure with dry nitrogen.)

Figure 2a shows maps of four elements in a hemisected frozen rat eye. The smooth distribution of electrolytes in the aqueous humor of the anterior chamber, which would be altered or lost with other preparative techniques, is preserved in this frozen hydrated specimen. The high sulfur concentration of the lens, which is rich in glutathione and other sulfur-containing peptides and proteins, can be clearly seen. The sulfur concentration is not uniform across the lens but reaches a maximum at the center with a corresponding minimum in the potassium content. Areas of relatively high calcium concentration are seen in the region of the supporting ligaments of the lens. Figure 2b is a line scan parallel to the optic axis of the same eye from retina to cornea, demonstrating the dramatic rise in the sulfur content of the lens with a simultaneous minimum in the potassium content; since the proton microprobe penetrates the specimen only to a depth of 25 to 50 μm, these variations reflect true differences in local concentration in the cortex and nucleus of the lens, rather than the greater thickness of lens tissue underlying the middle of the section. The average chlorine concentration is higher in the anterior than in the posterior chamber of the eye, consistent with earlier observations of lower contents of chloride in the posterior chambers of animals with relatively large lenses (*11*).

We also used the cold stage to study kidney specimens from rats producing concentrated urine. Kidneys were removed and immersed in isopentane at −160°C within a few seconds. Sections were then shaved from the specimens in a refrigerated microtome to obtain a cross section of cortex, outer and inner medulla, and papilla on the exposed surface. Figure 3 shows the distribution of chlorine and potassium in the shaved blocks, corresponding to a horizontal section of the kidney. Chlorine is concentrated in the inner medulla and papilla, reflecting the countercurrent concentration and exchange mechanisms of the kidney. This represents the first visualization of the elemental gradient in the concentrating kidney. A line scan of chlorine (as in Fig. 2b) verifies that the chlorine content rises abruptly at the boundary between the outer and inner medulla and maintains a relatively constant elevated concentration throughout the papilla. This observation confirms earlier electron microprobe results and is consistent with a recently proposed interpretation of the renal countercurrent mechanism (*12*). The potassium content, by contrast, does not rise in the papilla (*13*).

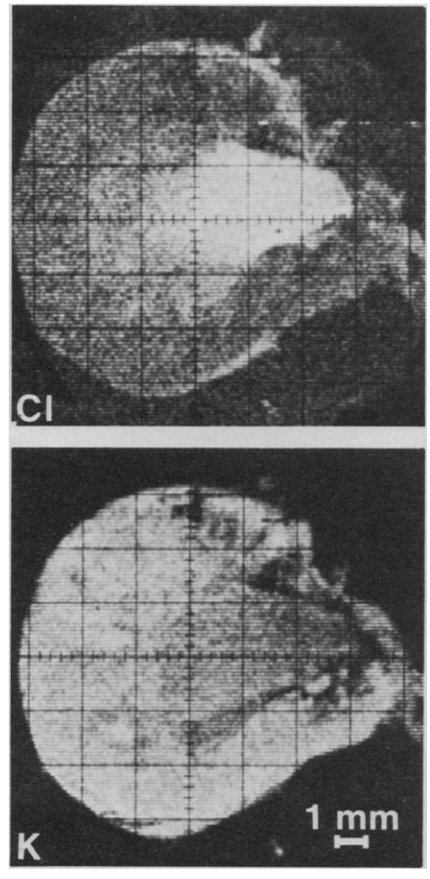


Fig. 3. Distribution of chlorine and potassium in frozen hydrated rat kidney. The triangular region rich in chlorine is the renal papilla; exposure, 10 minutes.

These results reflect a few of the possible applications of the proton microprobe to problems in biology and medicine. Although such an instrument is not yet commercially available, its unique capacity for high-sensitivity x-ray elemental analysis (even at trace concentrations) of arbitrarily large specimens in an atmospheric environment, allowing convenient study of frozen hydrated samples, provides the capability to study a

multitude of problems of current interest which are impractical by other techniques.

PAUL HOROWITZ
MICHAEL ARONSON
*Department of Physics,*
*Harvard University,*
*Cambridge, Massachusetts 02138*
LEE GRODZINS
WILLIAM LADD
*Department of Physics,*
*Massachusetts Institute of Technology,*
*Cambridge 02139*
JEAN RYAN
*Lincoln Laboratory, Massachusetts*
*Institute of Technology, Lexington 02173*
GEORGE MERRIAM
CLAUDE LECHENE
*Department of Physiology,*
*Harvard Medical School,*
*Boston, Massachusetts 02115*

### References and Notes

1. P. Horowitz and L. Grodzins, *Science* **189**, 795 (1975).
2. W. A. Dewar and J. M. A. Lenihan, *Scot. Med. J.* **1**, 236 (1956); L. Magos and T. W. Clarkson, *J. Assoc. Off. Anal. Chem.* **55**, 966 (1972); F. K. Paddock, C. C. Loomis, A. K. Perkons, *New Engl. J. Med.* **282**, 784 (1970).
3. L. Zeitz, R. Lee, E. O. Rothschild, *Anal. Biochem.* **31**, 123 (1969); P. Horowitz and J. A. Howell, *Science* **178**, 608 (1972).
4. Proton-induced x-ray analysis has been used to study aligned multiple strands of hair at low resolution (1 cm) (see R. K. Jolly, G. Randers Pehrson, S. K. Gupta, D. C. Buckle, H. Aceto, Jr., paper presented as part of the Proceedings of the 3rd Conference on Applications of Small Accelerators, 21–23 Oct. 1974, Denton, Texas).
5. T. Giovanoli-Jakubczak and G. G. Berg, *Arch. Environ. Health* **28**, 139 (1974).
6. D. D. Munro, *Arch. Dermatol.* **93**, 119 (1966).
7. F. Bakir *et al.*, *Science* **181**, 230 (1973); T. W. Clarkson (University of Rochester) provided the hair of the methylmercury victim—series 214, family 29; J. A. Swift (Unilever Research, England) provided the arsine victim's hair.
8. Measured by C. A. Pounds, Home Office Central Research Establishment, Aldermaston, England.
9. A. C. Alfrey, L. L. Nunnelley, H. Rudolph, W. R. Smythe, paper presented as part of the Proceedings of the 24th Annual Denver X-ray Conference, 1975.
10. C. P. Lechene, T. Strunk, R. Warner, C. Conty, in *Proceedings of the Microbeam Analysis Society, 10th Annual Conference* (Microbeam Analysis Society, Bethlehem, Pa., 1975), pp. 49a–49e.
11. H. Davson, *The Physiology of the Eye* (Academic Press, New York, 1972), pp. 38–39.
12. J. V. Bonventre and C. P. Lechene, *Kidney Int.* **8**, 469 (1975); C. P. Lechene and J. V. Bonventre, in *Proceedings of the Microbeam Analysis Society, 11th Annual Conference* (Microbeam Analysis Society, Bethlehem, Pa., in press)
13. When interpreting proton microprobe scans, it must be kept in mind that the x-ray continuum background may sometimes be nonnegligible; therefore, variations in the various elemental signals are of the most significance, while low steady signals may have some background contribution. In the eye and kidney scans, for instance, the ratio of elemental signal to continuum background was typically in the range of 3:1 to 30:1.
14. We thank J. A. Swift and T. W. Clarkson for providing hair specimens. We thank H. Rosen for operating the proton accelerator. This work was supported with funds from the National Science Foundation (grant PCM-74-23522 A01), the Energy Research Development Administration [contract E(11-1)-3069], the National Institutes of Health (grants R01-HL-15552 and P07-RR-00679), and the Department of the Air Force.

21 June 1976; revised 30 August 1976

# Titanium(III) Citrate as a Nontoxic Oxidation-Reduction Buffering System for the Culture of Obligate Anaerobes

Abstract. *An oxidation-reduction buffering system based on titanium(III) citrate eliminates any traces of oxygen in a culture medium, serves as an indicator for low oxidation-reduction potentials, and prevents the growth of facultative anaerobes, which frequently contaminate anaerobic cultures.*

As shown by Hungate (*1*), it is practically impossible to prepare media with a low oxidation-reduction potential for the culture of anaerobic bacteria only by removing all traces of oxygen. A reducing agent has to be added, and sulfide, cysteine, and thioglycolic acid are commonly used for this purpose. These chemicals have disadvantages, however, such as toxicity for microorganisms at fairly low concentrations, and slow reaction rates in the presence of traces of oxygen that find access into the culture vessels.

Titanium(III), well known in inorganic chemistry as a strong reducing agent, was found to be applicable also in microbiology (Fig. 1). At the normally neutral conditions of culture fluids, $Ti^{3+}$ precipitates as a hydroxide [the solubility product of $Ti(OH)_3$ is about $10^{-40}$ (*2*)]. However, this can be avoided by adding citrate as a complexing agent (*3*). The titanium(III) citrate complex forms a blue-to-violet solution, which is decolorized on oxidation. Consequently, this complex also serves as an oxidation-reduction indicator. Its equilibrium potential at $p$H 7 is $E_H^0 = -480$ mv (*4*). Autoxidation of titanium(III) eliminates oxygen from a growth medium (*5*) by a first-order reaction with a rate constant of $k = (11.4 \pm 0.8) \times 10^{-5}$ sec$^{-1}$ at 25°C (*6*).

We examined possible growth inhibitions or other detrimental effects on anaerobic microorganisms by large concentrations of titanium(III) citrate. The following physiologically different organisms were investigated: *Methanobacterium* strain AZ (DSM 744) (*5*), an extremely anaerobic organism; *Clostridium formicoaceticum* (DSM 92), a strict

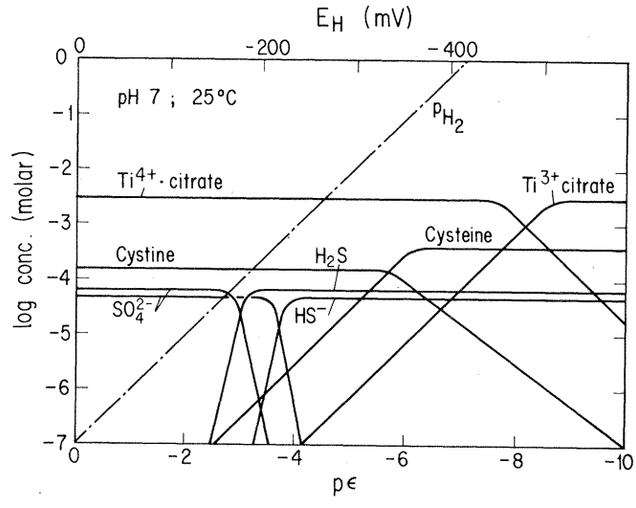


Fig. 1 (top right). Equilibrium concentrations of pertinent oxidation-reduction compounds as a function of $E_H$ or the relative electron activity ($p\epsilon = -\log [e^-]$) at $p$H 7.0 and 25°C. This equilibrium diagram has been calculated by using standard equilibrium constants (*2, 4, 10*). The concentrations of the four reducing agents ($H_2$, $Ti^{3+}$ citrate, cysteine, and $HS^-/H_2S$) represent the conditions under which no inhibition of the growth of *Methanobacterium* strain AZ was observed (*5*). The polarographically active $Ti^{4+}$ citrate complex is stoichiometrically not identical with the $Ti^{3+}$ citrate complex (*9*). Reduction of water to hydrogen by the latter was not detected. Fig. 2 (bottom right). Growth rates, at different $Ti^{3+}$ citrate concentrations, of *Clostridium formicoaceticum* (DSM 92), $p$H 8.0; *Bifidobacterium bifidum* (DSM 20 215), $p$H 6.8; and *Methanobacterium* strain AZ, mineral medium + cysteine hydrochloride (0.05 g/liter) and yeast extract (2 g/liter) (*5*), $p$H 7.0. The temperature was 33°C. The increase of the growth rate of *C. formicoaceticum* and *B. bifidum* at low $Ti^{3+}$ citrate concentrations is due to the reduction of organic components in the complex organic media. This is indicated by fading of the dark brown color of the solutions.